Dalton Transactions

Accepted Manuscript

ROYAL SOCIETY OF CHEMISTRY

www.rsc.org/dalton

Newly synthesized Ru(II)/Os(II)-polypyridyl complexes with pendent acetyleacetone functionality for coupling to nanoparticulate TiO_2 surfaces and studies on interfacial electron transfer dynamics

*Tanmay Banerjee,[§$] Abul Kalam Biswas,[†¶] Tuhin Subhra Sahu,[†] Bishwajit Ganguly,*[†¶] Amitava Das,*[§$] and Hirendra Nath Ghosh *[‡]*

[§] *CSIR-National Chemical Laboratory, Pune-411008, India.*

[†] *CSIR-Central Salt and Marine Chemicals Research Institute, Bhavnagar-364002, India.*

[‡] *Radiation and Photochemistry Division, Bhabha Atomic Research Centre, Mumbai, 400085, India.*

[$] *Academy of Scientific and Innovative Research, CSIR-National Chemical Laboratory, Pune-411008, India.*

[¶] *Academy of Scientific and Innovative Research, CSIR-Central Salt and Marine Chemicals Research Institute, Bhavnagar, Gujarat-364002, India.*

* To whom correspondence should be addressed. E-mail: hnghosh@barc.gov.in (HNG), Fax: (+) 91-22-25505331/25505151, a.das@ncl.res.in (AD), Fax: 00-91-20-25902629, ganguly@csmcri.org (BG), Fax: 00-91-278-2567562.

Abstract:

New Ru(II)- and Os(II)-polypyridyl complexes have been synthesized with pendent acetylacetone (acac) functionality for anchoring on the nanoparticulate TiO_2 surfaces with an aim to develop an alternate sensitizer molecule that could be utilized for designing an efficient dye sensitized solar cell (DSSC). Time-resolved transient absorption spectroscopic studies in the femtosecond time domain have been carried out. The charge recombination rates are observed to be very slow as compared to those for strongly coupled dye molecules having catechol as the anchoring functionality. Results of such studies reveal that the electron injection rates from the metal complex based LUMO to the conduction band of the TiO_2 are faster that one would expect for analogous complex in which the chromophoric core and the anchoring moiety is separated with multiple saturated C-C linkages. Such an observation is rationalized based on the computational studies and a relatively smaller spatial distance between the dye LUMO and the TiO_2 surface is accounted for this. Results of this study are compared with those for analogous complexes having *gem-dicarboxy* group as the anchoring functionality for covalent binding to TiO_2 surface in order to compare the role of binding functionalities on electron transfer dynamics.

Introduction:

Dye sensitized solar photovoltaic and fuel cells have drawn enormous recent attention as probable cost effective alternative to conventional solar light harvesting architectures.[1] Consequently, the last few years have witnessed insurgent research efforts towards maximization of the efficiency of such devices. In order to achieve this, many factors need to be optimized.[1d,f] Likewise, it is very important to have novel anchoring units for pH stable binding of sensitizer dyes to TiO_2 in aqueous solutions.[2a] This question of pH stability of the sensitizer dyes in aqueous solutions of high pH arises because of the low ground state pKa of carboxylic acids that causes surface de-chelation at pH greater than about 4 – 4.5.[2a] In the recent past, quite a number of new anchoring units have been proposed thus, in order to overcome this problem.[2b-f]

The pH sensitivity of carboxylate mode of binding is perhaps its only noteworthy demerit. The fact that such binding modes have ruled the dye solar research ever since the inception of the concept in 1991 arises perhaps because of their high equilibrium binding constants and high saturation surface coverages, facile synthetic routes and perhaps most importantly,

optimal interfacial electron transfer rates. Thus, while designing new anchoring moieties which can possibly overcome the problem associated with the stability of the dye-TiO_2 linkage in aqueous solutions, a compromise in any of the aforesaid factors would certainly not be judicious. Such is the case with many of the proposed alternatives, namely, catecholates,[2c] resorcinolates,[2d] and there are only a few anchoring groups eg. hydroxamates[2f] that meet all the criteria for a successful linkage .

The present article deals with another such, but not exhaustively explored anchoring unit, acetylacetone. Such anchoring units have been shown to have high water resistance and oxidative stability.[3a] Meyer and co-workers in the year 1996 explored the possibility of using a β-ketoester moiety for anchoring functionality on TiO_2 surfaces and reported photoinduced process in the nano-second time domain.[2e] Futher studies were carried out by Batista and co-workers with Mn(II)-terpyridine acetylacetone complexes and very recently on coumarine moieties.[3a,b] Binding of an un-substituted acac on ZnO surfaces was explored by Baher *et al.,*[3c] while Warnan *et al.* reported studies on photocurrent generation efficiency for a Ru(II)-based sensitizer having 2,2'-bipy moiety, substituted with an acac functionality for anchoring on ZnO surfaces.[3d] Synthesis of different acac-linked BODIPY dyes have been reported by Ziessel and co-workers for tuning the absorption spectral wavelength.[3e] More recently, Mallouk and his co-workers have reported use of a heteroleptic Ru(II)-polypyridyl complex with a pendent malonate group for modifying the IrO_2 surfaces and this was responsible for facilitating the hole migration process for favouring the subsequent catalytic water splitting.[3f]

In one of our very recent reports, we studied *geminal* dicarboxylic acids bound Ru(II)-polypyridyl dyes on TiO_2,[4] where the binding *geminal* dicarboxylic acid unit was separated from the chromophoric unit by multiple saturated spacers, still electron injection rate was found to be sub 400 fs[4]. Interestingly back electron trasfer found to be very slow.

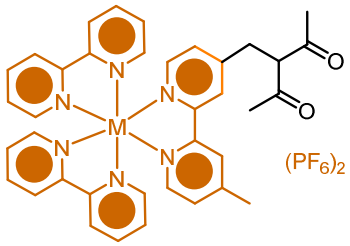

M = Ru^{2+}, **3**
= Os^{2+}, **4**

Scheme 1. Structure of the Ru(II)- and Os(II)-based dye molecules **3** and **4**, respectively.

With this knowledge, similar acetylacetone based Ru(II)- and Os(II)-polypyridyl complexes, **3** and **4**, respectively, where the binding unit and the sensitizer core are separated by exactly the same number of saturated spacers, have been synthesized. The interfacial electron transfer rates have been accurately quantified by femtosecond transient absorption spectroscopic studies and are the focus of the present study.

Meyer and co-workers, in one of their earlier reports had described using an acetyl ester functionality of the on Ru(II)-polypyridyl dye for anchoring on the semiconductor surfaces,[2e] and had used a laser pulse having 8 ns full width at half- maximum (fwhm). Results of our previous study tend to suggest[4] that the electron injection processes could be much faster and may actually happen within a much shorter time scale. For the Mn(II)-terpyridine acetylacetone complex carried out by Batista and co-workers,[3a] a ~500 fs resolution pulse was used to excite the samples in a terahertz spectroscopy experiment and so their photoinjection process was also limited by the width of the laser pulse. In this study, the interfacial electron transfer processes had only been grossly indentified and the dynamics was not discussed in detail. Also, in the recently studied coumarine-acetylacetone based sensitizer, again studied by Batista and co-workers,[3b] the electron injection was only theoretically predicted to be ultrafast.

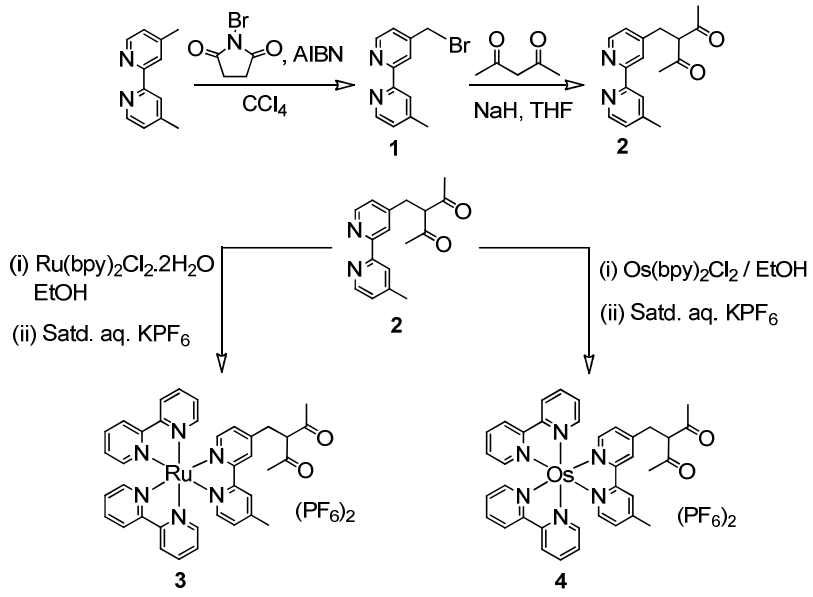

Scheme 2. Methodologies that are used for the synthesis of complexes **3** and **4**.

In view of these facts, the present femtosecond pump-probe spectroscopic study has enabled us to compare the results with those of our previous studies having *gem*-dicarboxylic acid as the anchoring functionality and thus to quantify the influences of the subtle changes in anchoring functionality on interfacial electron transfer dynamics in dye-spacer-semiconductor configuration. Such results have relevance in developing a better insight and understand the efficacy of designing new dye molecule for use in the *dye-spacer-anchor* arrangement for a possible development of novel sensitizer systems.

Materials and methods:

a. Materials: $Ti(OCH(CH_3)_2)$ (97%), $(CH_3)_2CHOH$, 4,4'-dimethyl-2,2'-bipyridine, 2,2'-bipyridine, $RuCl_3.xH_2O$, $(NH_4)_2OsCl_6$, N-bromosuccinimide (NBS), NaH, NH_4PF_6 and KPF_6 are acquired from Sigma-Aldrich and used as received. All other reagents (AR grade; S.D. Fine Chemicals, India) have been used without any further purification. Various solvents (CCl_4, $CH_3C_6H_5$, $(CH_3)_2CO$, CH_2Cl_2, tetrahydrofuran (THF), CH_3OH, C_2H_5OH and CH_3CN) have been dried and distilled prior to use for the present study. Nanopure water (Barnsted System, USA) has been used for making all aqueous solutions. Solvents are typically degassed thoroughly with IOLAR grade dinitrogen gas before use in the preparation of standard solutions. $Ru(bpy)_2Cl_2$[5] and $Os(bpy)_2Cl_2$[6] have been prepared following previously reported procedures. Synthesis of the intermediate reagent, 4-(bromomethyl)-4'-methyl-2,2'-bipyridine is achieved in reasonable yield (30%, calculated based on the reactants used for the reaction) following a previously reported procedure.[4]

b. Analytical Methods: Elemental analyses (C, H, N) are carried out using a Perkin-Elmer 4100 elemental analyzer; while pH titrations carried out on a Mettler Toledo S20 pH meter. Perkin-Elmer Spectra GX 2000 spectrometer has been used for been recorded FTIR spectra as a KBr pellets in a cell fitted with a KBr window. ^1H NMR spectra are recorded on a Bruker 200/500 MHz FT-NMR (Model: Avance-DPX 200/500) using tetramethylsilane (TMS) as an internal standard. ESI-Ms measurements are carried out on a Waters QTof-Micro instrument. Uv-vis spectra have been recorded with a Varian Cary 500 UV-Vis-NIR spectrophotometer and steady state luminescence spectra at room-temperature have been recorded with Edinburgh FS P920 luminescence spectrofluorimeter, fitted with a red-sensitive photomultiplier tube. Potential value for redox couples are evaluated using a

bipotentiostat (AFCPBI, PINE Instrument Co.) electrochemical instrument with a conventional three-electrode cell assembly. An Ag/AgCl (non-aqueous) an auxiliary, a platinum as electrode and a saturated KCl as reference electrode have used for all measurements. Ferrocene (Fc) has been used as an internal standard; while all potentials values are quoted with respect to the Normal Hydrogen Electrode (NHE) in water.[7]

c. Femtosecond Visible Spectrometer: The tuneable visible spectrometer with 50 femtosecond pulse width has been developed based on a multipass amplified femtosecond Ti:sapphire laser system supplied by Thales, France and details of the configuration of such instrument, along with the energy used for pump probe pulses are provided in supporting information.[8]

d. Preparation of sample solutions: Complexes discussed (**3**, **4**, **5** and **6**) are initially dissolved in minimum volume of acetonitrile and this solution was further diluted with water in such way that the acetonitrile content in the homogeneous solution of such complexes is ~1%. Then such dye solution is added into the aqueous colloidal dispersion of the nanoparticles with constant stirring over a period of 15 minutes. Thus, effective acetonitrile content is such solution is typically less than 1% and such solution is abbreviated as water through the text. The resulting solutions are stirred for half an hour and then kept in dark for 18 hours at room temperature for efficient binding of the dye molecules to the TiO_2 surfaces. All sample solutions are deoxygenated by bubbling high purity nitrogen (99.95 IOLAR grade from Indian Oxygen Co. Ltd., India and saturated with water vapour) through the solutions.

e. Synthesis of TiO_2 nanoparticles: TiO_2 nanoparticles have been obtained from a previous study and are provided in the supporting information.[2d] All colloidal samples (15 g/L) have been prepared for the present study by following a previously reported procedure.[9]

f. Computational Methodologies: All calculations have been performed with density functional program package DMol[3] in Materials Studio (version 4.1) of Accelrys Inc.[10] The optimization of additive on the TiO_2–surface was carried out with LDA/PWC/DND level of theory. The frontier molecular orbitals calculations have been performed with GGA/PBE/DNP level of theory using the optimized geometries.[11] The solvent effect in these calculations have been employed using the dielectric constant of water (dielectric constant = 78.54) using the COSMO model.[12] The size of the DND basis is comparable to Gaussian 6-31G* basis sets, and DNP basis sets are comparable to 6-31G** sets. However, the numerical basis set is much more accurate than a Gaussian basis set of the similar size.[13] Furthermore,

the numerical basis sets are free of basis set super-position error (BSSE).[10,13] The computational performance is improved by a Fermi smearing of 0.002 hartree (1 Ha = 27.212 eV) and a global cutoff of 4.5 Å. We have employed the tolerance of the energy, gradient, and displacement convergences are 2×10^{-5} Ha, 4×10^{-3} Ha.Å^{-1} and 5×10^{-3} Å respectively.[14] In this study we have used the reported titanium dioxide cluster [Ti_8O_{32}] for the TiO_2 anatase {101} surfaces.[15] The cluster has been made neutral charge by adding hydrogen atoms on oxygen atoms with dangling bonds.

g. Synthesis:

i. 4-(bromomethyl)-4'-methyl-2,2'-bipyridine (1): This reagent used as an in intermediate for synthesis of **2** is prepared and purified following reported procedure.[4] Analytical and spectroscopic data for this purified reagent **1** agree well for the desired purity of this reagent. ESI-MS (*m/z*): Calculated for $C_{12}H_{11}BrN_2$ is 262.01, Observed is 263.01 $[M + 1]^+$; ^{1}H NMR (500 MHz, $CDCl_3$): δ (ppm) 8.67 (1H, d, J = 5.2 Hz, H^6 (bpy)); 8.55 (1H, d, J = 5.2 Hz, $H^{6'}$ (bpy)); 8.4 (1H, s, H^3 (bpy)); 8.22 (1H, s, $H^{3'}$ (bpy)); 7.35 – 7.33 (1H, m, H^5 (bpy)); 7.16 (1H, d, J = 5.2 Hz, $H^{5'}$ (bpy)); 4.49 (2H, s, –CH_2Br); 2.44 (3H, s, bpy–CH_3). IR (KBr pellet, cm^{-1}) 1199 (ν_{bend} (C–Br)). Elemental Analysis: Calculated for $C_{12}H_{11}BrN_2$ is C 54.77, H 4.21, N 10.65; Found is C 54.75, H 4.24, N 10.61.

ii. 3-((2-(4-methylpyridin-2-yl)pyridin-4-yl)methyl)pentane-2,4-dione (2): Acetylacetone (0.15 ml, 1.47 mmol) is added slowly with constant stirring to a dry THF solution (~10 ml) of NaH (50%, 70 mg, 1.47 mmol), maintained at 0ºC. After completion of this addition, resulting turbid suspension is allowed to equilibrate for 15 min and to this, a 10 ml THF solution of **1** (386 mg, 1.47 mmol) is added drop-wise over a period of 20 minutes. The reaction mixture is then stirred at room temperature for one complete day. All such procedures are performed strictly under positive pressure of dinitrogen gas. Then ~2 ml of water is added to the reaction mixture and stirred for 5 minutes to ensure the decomposition of excess NaH that could still be present in the reaction medium. THF is then evaporated under reduced pressure and crude reaction product is extracted into the chloroform layer by solvent extraction. This chloroform solution was then evaporated to dryness to isolate the crude product and is further purified by column chromatography using silica gel 200-400 mesh as stationary phase and $CHCl_3$/CH_3OH as the eluent. Reagent **2** was isolated as a pale yellow solid (Yield: 310.5 mg, 75%). ESI-Ms (*m/z*): Calculated for $C_{17}H_{18}N_2O_2$ is 282.14, Observed is 283.16 $[M + H]^+$; ^{1}H NMR (500 MHz, CD_3CN): δ (ppm) 8.54 – 8.48 (2H, m, H^6

(bpy), $H^{6'}$ (bpy)); 8.26 – 8.22 (2H, m, H^3 (bpy), $H^{3'}$ (bpy)); 7.21 – 7.19 (2H, m, H^5 (bpy), $H^{5'}$ (bpy)); 4.30 (1H, t, J = 7 Hz, -CH-CH_2); 3.16 (2H, d, J = 7 Hz, -CH-CH_2); 2.41 (3H, s, bpy-CH_3); 2.16 (6H, s, -$COCH_3$). IR (KBr pellet, ν (cm^{-1})): 2924 (sp^2 C-H), 1744 (C=O). Elemental Analysis: Calculated for $C_{17}H_{18}N_2O_2$ is C 72.32, H 6.43, N 9.92; Found is C 72.30, H 6.40, N 9.97.

iii. {bis-(2,2′-bpy)-(3-((2-(4-methylpyridin-2-yl)pyridin-4-yl)methyl)pentane-2,4-dione)} ruthenium(II) hexafluorophosphate (3): Complex 3 is synthesized by reacting $Ru(bpy)_2Cl_2.2H_2O$ (200 mg, 0.3846 mmol) and **2** (108.5 mg, 0.3846 mmol) in ~30 ml of ethanol for 8 hours under refluxing condition with continuous stirring and inert atmosphere. Then the reaction is cooled to room temperature and solvent is reduced under vacuum to ~5 ml. To this concentrated solution, aqueous solution of excess NH_4PF_6 (10 mole equivalents) is added and stirred at room temperature for 15 min. This is further kept at ~8ºC for 5 hours to ensure the complete precipitation of the desired Ru(II)-polypyridyl complex as the hexafluorophosphate salt. This red precipitate is collected through filtration, washed with large volumes of cold water and dried in a vacuum desiccator. The crude compound so obtained is purified by column chromatography using a silica gel column (100-200 mesh) and acetonitrile/water/saturated aqueous KPF_6 (98:1.8:0.2; v/v/v) as the eluent. Major fraction is collected and the solvent is removed to isolate a red solid. Excess KPF_6 that could be present in this solid is partitioned into the aqueous layer after using a predominantly dichloromethane solution (CH_2Cl_2:CH_3CN, 98:2 (v/v)) of this red solid for solvent extraction. The organic phase is dried over anhydrous sodium sulphate and is evaporated to dryness to give the desired product in pure form (Yield: 150 mg, 39.6%). ESI-MS (*m/z*): Calculated for $C_{37}H_{34}N_6O_2PF_6Ru$ – 841.1 $[M - PF_6^-]^+$, Observed 841.46 $[M - PF_6^-]^+$; ^{1}H NMR (500 MHz, CD_3CN): δ (ppm) 8.51 (4H, d, J = 8.5 Hz, H^6 (bpy) and $H^{6'}$ (bpy)); 8.41 – 8.38 (1H, m, H^3 (bpy-acac)); 8.06 – 8.03 (4H, m, H^3 (bpy) and $H^{3'}$ (bpy)); 7.74 – 7.71 (3H, m, H^6 (bpy-acac) and $H^{6'}$ (bpy-acac), $H^{3'}$ (bpy-acac)); 7.69 – 7.68 (1H, m, H^4 (bpy) or $H^{4'}$ (bpy)); 7.57 (1H, d, J = 5 Hz, H^5 (bpy-acac)); 7.54 (1H, d, J = 6 Hz, $H^{5'}$ (bpy-acac)); 7.41 – 7.37 (5H, m, H^5 (bpy) and/or $H^{5'}$ (bpy) and/or H^4 (bpy) and/or $H^{4'}$ (bpy)); 7.25 – 7.22 (2H, m, H^5 (bpy) and/or $H^{5'}$ (bpy) and/or H^4 (bpy) and/or $H^{4'}$ (bpy)); 4.38 (1H, t, J = 7 Hz, -CH-CH_2); 3.22 (2H, d, J = 7.5 Hz, -CH-CH_2); 2.55 (3H, s, bpy-CH_3); 2.19 (6H, s, -$COCH_3$). IR (KBr pellet, cm^{-1}) 1708 (ν(C=O)), 840 (ν(PF_6)). Elemental Analysis: Calculated for $C_{37}H_{34}N_6O_2P_2F_{12}Ru$ is C 45.08, H 3.48, N 8.53; Found is C 45.0, H 3.55, N, 8.52.

iv. {bis-(2,2′-bpy)-(diethyl 2-((4'-methyl-2,2'-bipyridin-4-yl)methyl)malonate) osmium(II) hexafluorophosphate (**4**): This is prepared by a similar procedure as adopted for the synthesis of **3**, except $Os(bpy)_2Cl_2.2H_2O$ (200 mg, 0.328 mmol) and **2** (114 mg, 0.333 mmol) are refluxed in ethanol instead of $Ru(bpy)_2Cl_2.2H_2O$ and **2** (108.5 mg, 0.3846 mmol). However, the purification procedure adopted is different. The crude compound so obtained is purified by column chromatography over neutral alumina using acetonitrile/toluene (1:1, v/v) as the eluent. The last fraction (major fraction too) is collected and the solvent is removed to isolate a greenish-black solid (Yield: 196 mg, 52.5%). ESI-Ms (*m/z*): Calculated for $C_{37}H_{34}N_6O_2PF_6Os$ 931.16 $[M - PF_6^-]^+$, Observed 931.80 $[M - PF_6^-]^+$. ^1H NMR (200 MHz, CD_3CN): δ (ppm) 8.45 (4H, d, J = 8 Hz, H^6 and $H^{6'}$ (bpy)); 8.32 (2H, d, J = 6 Hz, H^6 and $H^{6'}$ (bpy-acac)); 7.87 – 7.79 (4H, m, H^3 and $H^{3'}$ (bpy)); 7.65 - 7.55 (4H, m, H^4 and $H^{4'}$ (bpy)); 7.47 – 7.41 (2H, m, H^3 and $H^{3'}$ (bpy-acac)); 7.33 – 7.23 (4H, m, H^5 and $H^{5'}$ (bpy)); 7.16 – 7.11 (2H, m, H^5 and $H^{5'}$ (bpy-acac)); 4.31 (1H, t, J = 7 Hz, -CH-CH_2); 3.25 (2H, d, J = 7.4 Hz, -CH-CH_2); 2.60 (3H, s, bpy-CH_3); 2.06 (6H, s, -$COCH_3$). IR (KBr pellet, cm^{-1}) 1710 (ν(C=O)), 839 (ν(PF_6)). Elemental Analysis: Calculated for $C_{37}H_{34}N_6O_2P_2F_{12}Os$ is C 41.34, H 3.19, N 7.82; Found is C 41.38, H 3.23, N, 7.75.

Results and Discussion:

The synthetic methodology adopted is shown in Scheme 2. 4-bromomethyl,4′-methyl-2,2′-bipyridine is obtained from 4,4′-dimethyl-2,2′-bipyridine using NBS as a brominating reagent following a free radical pathway. This is then subjected to a nulceophilic substitution reaction with the deprotonated form of acac to yield **2**. This is used for the synthesis of the respective complex, **3** and **4**.

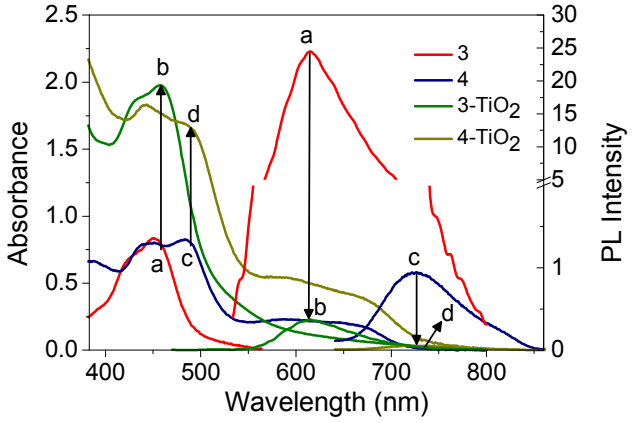

Figure 1: Absorption and steady state luminescence spectra of **3** (a), **4** (c), **3**-TiO_2 (b) and **4**-TiO_2 (d) in water. The concentrations of both complexes **3** and **4** are maintained at 5.0 x 10^{-5} M; while the concentration for TiO_2 is maintained at 15 g/L for all studies with TiO_2.

To understand charge trasfer behaviour for both the complexes **3** and **4** with TiO_2 nanoparticles it is very important to monitor both absorption and photoluminescence properties in absence and in presence of TiO_2 nanoparticles. Figure 1 depicts both steady absoprtion and photo-luminescence spectra for complexes **3** and **4** in absence and presence of TiO_2 nanoparticles. Both Complex **3** and **4** show optical absorption band peaking at 453 nm (ε = 1.63 x 10^4 M^{-1} cm^{-1}) and at 487 nm (ε = 1.68 x 10^4 M^{-1} cm^{-1}) which can be attributed to the $d_{M(II)} \rightarrow \pi^*_{bpy}$ [M = Ru(II)/Os(II)] based metal to ligand charge transfer (MLCT) transition.[22] For complex **4** in addition to the band at 487 nm an additional broad absorption between 550-710 nm (ε_{630} = 4400 M^{-1} cm^{-1}) appears which can be attributed to spin forbidden ^{3}MLCT based $d_{Os(II)} \rightarrow \pi^*_{bpy}$ transition. Now to comprehend charge trasfer interaction between the complexes and TiO_2 nanoparticles both in ground state and excited state we have carried out steady state optical absorption studies for both the complexes in presence of TiO_2 nanoparticles. It is clearly seen in Figure 1 that optical absorption for both complex **3** and **4** increases drastically on TiO_2 nanoparticle surface, which indicates significant interaction between the dye molecules and TiO_2 nanoparticles. However no red shifted absorption band maxima is observed. This observation indicates the weak electronic coupling between the dyes and nanoparticles similar to those reported for the conventional carboxylate bound dyes.[16,17] We also have carried out steady state emission measurements for both complexes **3** and **4** which show broad emission band peaking at 615 nm and 726 nm respectively which are attributed to ^{3}MLCT based emission. It is interesting to see that on exciting complex **4** at both 487 nm (^{1}MLCT band) and 630 nm (^{3}MLCT band), emission appears at only 650 -850 nm peaking at 726 nm. Now in presence of TiO_2 nanoparticles it is clearly seen that the emission intensity for both the dyes drastically reduced. This decrement of emission intensity can be attributed to electron injection from photo-excited complexes to TiO_2 nanoparticles.

To monitor interfacial electron trasfer reaction between complex **3**/**4** and TiO_2 nanoparticles it is very important know values of the redox potential of ground and excited state energy levels of the complex molecules. Potential data for the reversible Ru^{2+}/Ru^{3+} redox couple ($E_{1/2}$ = 1.26 V ($\Delta E = E_{PA} - E_{PC}$ = 74 mV) for complex **3** is evaluated using cyclic voltammometric studies (Figure 2). For complex **4**, the Os^{2+}/Os^{3+}-based reversible redox

couple appears at 0.8 V (ΔE = 71 mV) (Figure 2). These potential data are crucial in having a better insight and in understand the relative energy levels for the LUMO/excited state for the

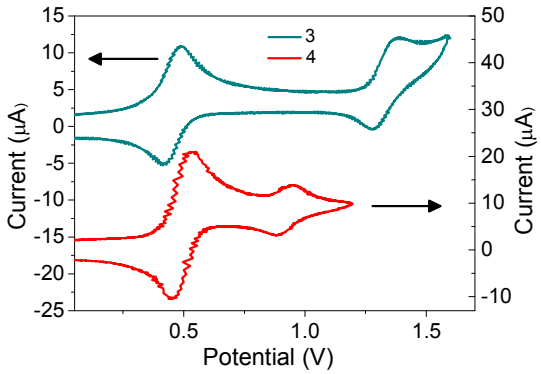

Figure 2. Cyclic voltammogram trace for complexes **3** and **4** in acetonitrile *vs.* Ag/AgCl, saturated KCl as the reference electrode (Scan rate of 100 mVs^{-1}) with Fc being used as an internal standard ($E_{1/2}$ for the Fc/Fc^{+} couple appears at < +0.5 V). Ligand based reductions are omitted since only the $M^{2+/3+}$ redox potentials have relevance in the interpretation of data throughout the manuscript.

complex molecules with respect to the conduction band of TiO_2 and thus having qualitative idea about the thermodynamic feasibility of electron injection from the dye LUMO to the conduction band of the semiconductor nanoparticles.

The $E_{0\text{-}0}$ values for the ^{1}MLCT states are approximated to be 2.50 eV and 2.31 eV for **3** and **4**, respectively, from the onset of optical absorption. This enabled us to evaluate the excited state potentials $E(S^+/S^*)$ data from the equation $[E(S^+/S^*)] = [E(S^+/S)] - E_{0\text{-}0}$ and thus, $E(S^+/S^*)$ values for the ^{1}MLCT states of complex **3** and complex **4** are found to be -1.24 V and -1.51 V, respectively. For the ^{3}MLCT states, the $E_{0\text{-}0}$ transition energy are calculated to be 2.34 eV and 1.89 eV, respectively, for **3** and **4**, from the respective excitation and emission spectra. The corresponding excited state potentials are thus -1.08 V and -1.09 V for **3** and **4**, respectively.[2d] The excited state potentials being above the conduction band level,[15] electron injection from the excited state of the sensitizers into the conduction band of TiO_2 becomes thermodynamically feasible.

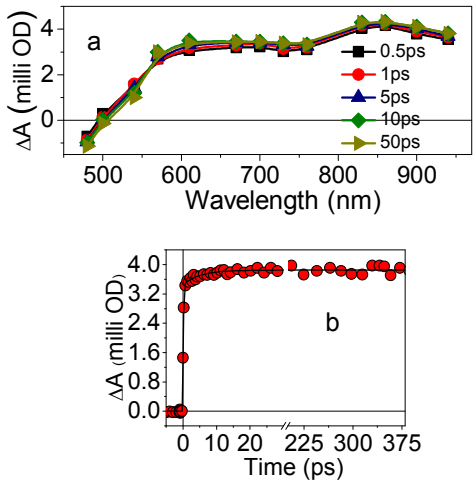

Figure 3: (a) Transient absorption spectrum of **3** at different delay times in water measured after 400 nm (fwhm < 120 fs) excitation. Concentration of **3** is ~ 200 μM, (b) the kinetic trace for **3** monitored at 940 nm.

To understand ultrafast electron transfer dynamics of complex **3** and **4** on TiO_2 nanoparticles surface it is important to study excited state dynamics of free sensitizers in absence of nanoparticles. Femtosecond transient absorption studies have been carried out for both the dyes and are showns in Figures 3 and 4, respectively. Figure 3 depicts the transient spectra of complex **3** which shows broad transient absorption band in 500-950 nm region and negative absorption (bleach) below 500 nm. The positive absorption band can be attributed to excited triplet state absorption[2d]. Recently Chergui *et al.* [20] employed broadband fluorescence spectroscopy and revealed that intersystem crossing in ruthenium polypyridyl complexes occurs in 15 ± 10 fs. So it is expected that in the present investigation at early time scale the transient absorption of the complex 3 are indeed due to triplet state.

To understand excited dynamics the transient at 900 nm was monitored and the kinetic trace was fitted bi-exponential growth with time constants of < 120 fs (89.6%) and 5 ps (10.4%). The initial ultrafast rise can be attributed to population due to the hot excited state[2d] and the slower 5 ps component might be arising due to vibrational cooling of the hot excited state[2] or interligand electron redistribution following excitation with 400 nm light (λ_{max}^{MLCT} for **3** is 453 nm) which distributes the electronic excitation over all the three bipyridine ligands.[2d,21] Such an assignment is corroborated by works carried out by Kelly and co-workers and Kohler and co-workers.[22] However such assignment was contradicted by many reports. Recent reports suggest that after one picosecond, the molecule has no recollection of which bipyridine was initially photoexcited.[23a] Chergui and co-workers reported the presence of 15

ps component which they did not attributed to abovementioned interligand electron redistribution.[23b] This component was proposed to be originating from restructuring of solvent molecules inserted amid the ligands and lying close to the metal center. Finally the long component (> 400 ps) can be attributed to excited state triplet state life time. Excited state life time of MLCT state of Ru(II)-polypyridyl complexes are known to be > 100 ns.

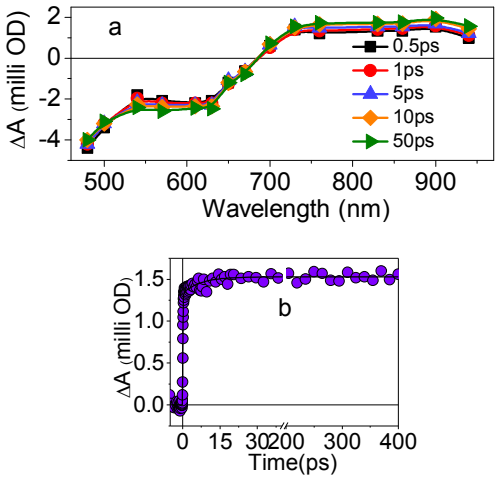

Figure 4: (a) Transient absorption spectrum of **4** at different delay times in water measured after 400 nm (fwhm < 120 fs) excitation. Concentration of **4** is ~ 200 μM, (b) The kinetic trace for **4** monitored at 900 nm.

Femtosecond transient absorption studies have also been carried out for complex **4** in water after exciting at 400 nm and shown in Figure 4. The transient absorption spectrum of **4** in water shows a broad positive absorption in the range 730-950 nm. Following the earlier arguments for complex **3**, this feature can be assigned to excited triplet state absorption. The negative absorptions at 480-550 nm and at 560-680 nm in the transient absorption spectrum of **4** can be assigned to bleach due to ^{1}MLCT and ^{3}MLCT ground state absorptions, respectively.[18a] The kinetic trace at 900 nm can be fitted with bi-exponential growth < 120 fs, (86.9%) and 7.2 ps (13.1%). The slower growth component can be attributed to vibrational cooling due to hot excited state or can be tentatively assigned to interligand electron redistribution in the ^{3}MLCT manifolds.

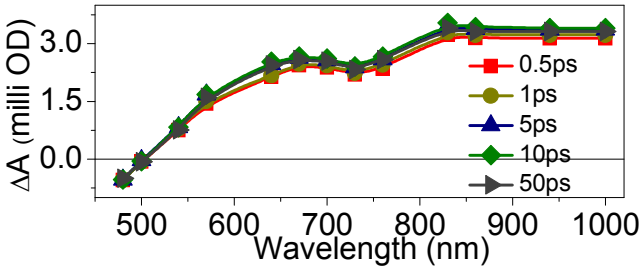

Figure 5: Transient absorption spectrum of **3**-TiO_2 at different delay times in water measured after 400 nm (fwhm < 120 fs) excitation. Concentration of **3** is ~ 200 μM while that of TiO_2 is 15 g/L.

Now to demonstrate interfacial electron transfer on TiO_2 nanoparticle surface in ultrafast time scale femtosecond transient absorption measurements have been carried out in TiO_2 nanoparticles after sensitizing with both complex **3** and **4** and shown in Figure 5 and Figure 6 respectively. Figure 5 shows the positive transient absorption in 520-950 nm region with two overlapping absorption band in 520-720 nm region attributed to transient band due to cation radical of complex 3 ($\mathbf{3}^{\bullet+}$) and 750-900 nm region attributed to transient band due to electron in the conduction band of TiO_2 nanoparticles. Assignment of cation radical was confirmed by complementary pulse radiolysis experiment where $\mathbf{3}^{\bullet+}$ is generated selectively by one electron oxidation reaction in presence of N_3 radical with **3** in N_2O-saturated aqueous solution (5% acetonitrile + 95% water) (Figure S1, Supporting Information). Assignment of 750-900 nm band is also corroborated by previous literature reports where it has been shown that electrons in the conduction band can be detected by visible, near IR and mid IR absorption.[2d,14,18,19a,24,25] In addition to broad positive absorption band, a negative absorption can be seen below 500 nm which can be attributed due to the bleach of ground state absorption.

Femtosecond transient spectra of complex **4** sensitized TiO_2 nanoparticles are demonstrated in Figure 6, which show two distinct absorption bands between 560-690 nm and 700-1000 nm in addition to a bleach due to ground state absorption below 550 nm. The first absorption band can again be assigned to the of cation radical of complex 4 ($\mathbf{4}^{\bullet+}$) which has been confirmed by our complementary pulse (Figure S1, Supporting Information). In our earlier investigation also it has been observed that cation radical absorption due to other osmium complexes[2d,18a] have huge overlap with ground state bleach like complex-**4**/TiO_2 system.

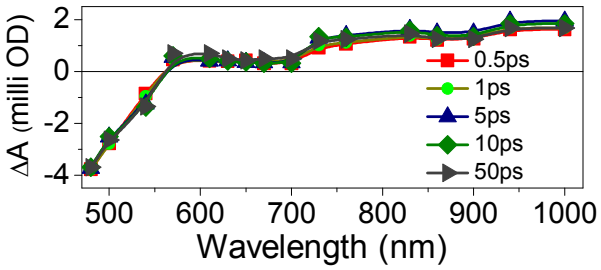

Figure 6: Transient absorption spectrum of **4**-TiO_2 at different delay times in water measured after excitation with 400 nm (fwhm < 120 fs) laser source. Concentration of **4** is ~ 200 μM while that of TiO_2 is 15 g/L.

Electron injection dynamics in both **3**-TiO_2 and **4**-TiO_2 systems was determined by monitoring the time of appearance of the electron signal at 1000 nm (Figure 7) and found to be bi-exponantial as shown in Table 1. In both cases the electron injection process found to take place with < 120 fs (pulse-width limited) and 1.2-1.4 ps. The pulse width limited component is attributed to electron injection from thermally unrelaxed singlet/triplet MLCT states.[26,27] However, the slower second component can be attributed to injection from

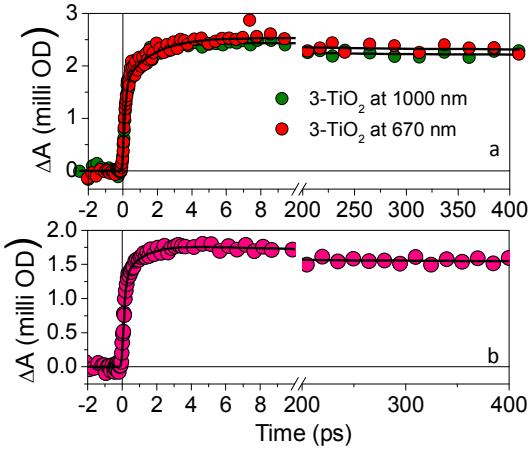

Figure 7: (a) Kinetic traces for **3**-TiO_2 and (b) **4**-TiO_2 at 1000 nm. The kinetic traces have been normalized with respect to the total signal amplitude.

thermalized ^{3}MLCT states.[26-29] To monitor injection dynamics cation radical signal at 670 nm for **3**-TiO_2 system has also been monitored and shown in Figure 7b and the kinetic data has been fitted with bi-exponential growth with time constants of <120 fs (+64.7%) and 1.7 ps (+35.3%) which found to match very close with that of electron signal at 1000 nm (Table 1). An amplitude-weighted-average-time constant (τ_{av}) for the injection processes in each of the aforesaid systems is calculated[30] and is shown in Table 1.

Table 1: Electron transfer parameters for **3**-TiO_2 and **4**-TiO_2 systems

System	Injection times (as monitored at 1000 nm)	Average injection time, τ_{av} *(fs)*	Decay times (as monitored at 1000 nm)	Recovery times for the signal at 480 nm
3-TiO_2	< 120 fs (67.3%), 1.4 ps (32.7%)	538	120 ps (10%), > 400 ps (90%)	120 ps (15%), >400 ps (85%)
4-TiO_2	< 120 fs (71.4%), 1.2 ps (28.6%)	430	12 ps (8.25%), 109 ps (6.73%), > 400 ps (85.02%)	12.5 ps (7.5%), 109 ps (5.5%), >400 ps (+87%)

It is clearly seen in Table 1 the average time constant for injection for both **3** and **4** are quite fast; much faster than expected for the dyes where the chromophore centre is separated from TiO_2 nanoparticles through anchoring unit by multiple saturated C-C linkages.[26,31] However, here the interesting fact is that the electron injection rate is about 2 times and 1.3 times slower, respectively, for the ruthenium and the osmium dyes, as compared to our previously studied *gem-dicarboxy* bound dyes, **5** and **6** (Scheme 3), for which the average injection lifetimes were recorded as 277.1 and 331.2 fs[4].

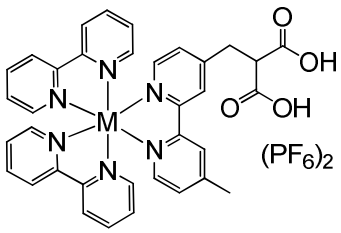

5, M = Ru^{2+}
6, M = Os^{2+}

Scheme 3: Structure of the Ru(II)- and Os(II) dye molecules **5** and **6**, respectively, used in our earlier work (Ref. 4) and results of which are being compared with those of complexes **3** and **4** in the present study.

The observed injection rates have been rationalized using frontier molecular orbitals calculated with (DFT) GGA/PBE/DNP level of theory. These calculated results showed that in the HOMO levels, significant electron densities residing on Ru(II) (**3**) (Figure 9) and on Os(II) (**4**). However, in LUMOs electron densities localized mainly on the unsubstituted bipyridine ligands instead of the bipyridine ligand attached with the anchoring acetylacetone

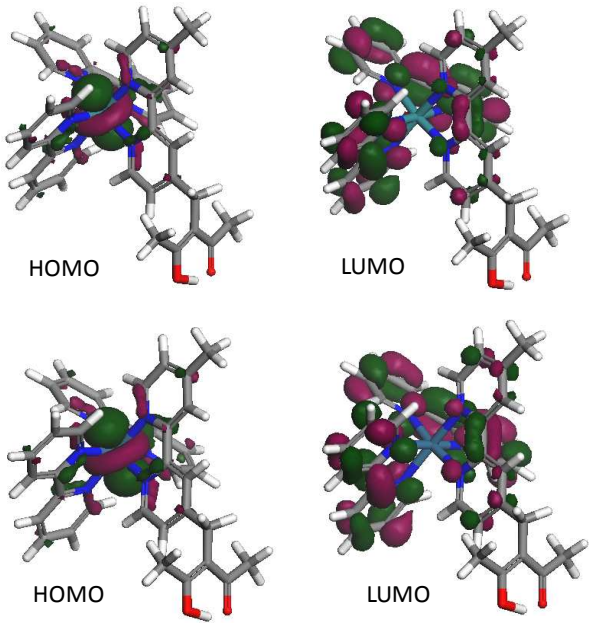

Figure 9: The calculated frontier molecular orbitals for **3** and **4** in water at GGA/PBE/DNP level of theory (white = hydrogen, gray = carbon, blue = nitrogen, red = oxygen and blue-green = ruthenium).

groups. To examine the frontier molecular orbitals of **3** and **4** anchored with the TiO_2 surface, {101} surface of anatase TiO_2 cluster was considered for DFT calculations. In the case of **3**- and **4**-TiO_2, the orbital coefficients calculated from the frontier molecular orbital are mostly localized on the metal center (HOMO−1) and the bipyridine ligand closer to the TiO_2 surface (LUMO+3) (Figure 10). In these cases, the dyes orients in such a way that one or both of the unsubstituted bipyridine moieties lie close to the semiconductor surface. Therefore, the electronic coupling of the dyes in excited state occurred through space or through bond by a superexchange tunnelling mechanism *via* the intervening solvent molecules with the Ti 3d conduction band.[25,30] This observation suggests that through space contributions may be responsible for the fast electron transfer from dyes **3** and **4** to TiO_2 surface instead of having multiple saturated linkers.[4] Incidentally, the optimized cluster geometry of **3**-TiO_2 shows that the distance between the TiO_2 surface and the middle point of the bipyridine ligand closer to the TiO_2 surface is 5.84 Å. This distance of closest approach was seen to be 4.70 Å for **5**-TiO_2. Thus, it seems that an increase of the distance between the LUMO electron density and the TiO_2 surface is manifested as slower electron injection rate in **3**-TiO_2 as compared to **5**-TiO_2.

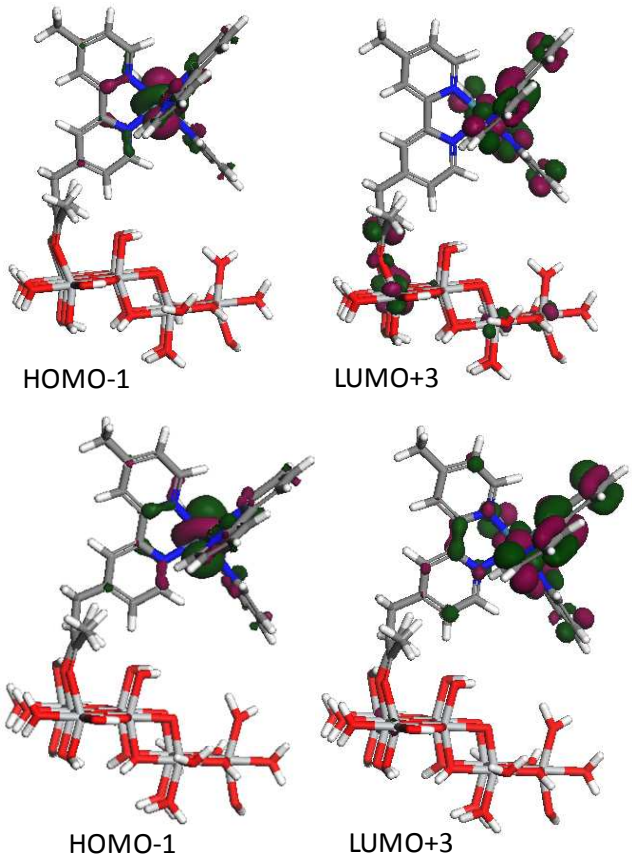

Figure 10: The calculated frontier molecular orbitals for clusters of **3**-TiO_2 and **4**-TiO_2 systems in water at GGA/PBE/DNP level of theory (white = hydrogen, gray = carbon, blue = nitrogen, red = oxygen, floral-white = titanium, and blue-green = ruthenium)

The abovementioned distance of closest approach is seen to be 5.76 Å for **4**-TiO_2 and thus the observed faster injection for **4**-TiO_2 than that in **3**-TiO_2 falls quite well in the line of our explanations. It must be noted that the difference in the calculated average injection times for **3**- and **4**-TiO_2 systems is 108 fs, very small for an excitation pulse width of ~ 120 fs and the difference in the distance of closest approach is also very small and only 0.08 Å.

It must however be noted that this comparison between **3**- and **5**-TiO_2 systems is only a very crude one. The reason is that the two systems involve two entirely different anchoring moieties. However, such a comparison has been made in light of the fact that the LUMO coefficients are completely localized in the unsubstituted bipyridine ligands both for the dyes **3** and **5** (Figure 8) and so conventional through bond electron injection pathway seems to be a very indifferent one.

Finally charge recombination (back electron transfer, BET) reaction were monitered after following the bleach recovery kinetics at 480 nm (Figure 10) and the fitting parameters are

shown in Table 1. BET dynamics found to be very slow in both the systems (**3**/TiO_2 and **4**/TiO_2) which is due to intervening saturated spacer groups between positively charged metal centre and the electrons located in the conduction band[2d], as a result higher charge separation has been observed. Such behaviour has been observed for many dye-semiconductor systems.[2e,26]

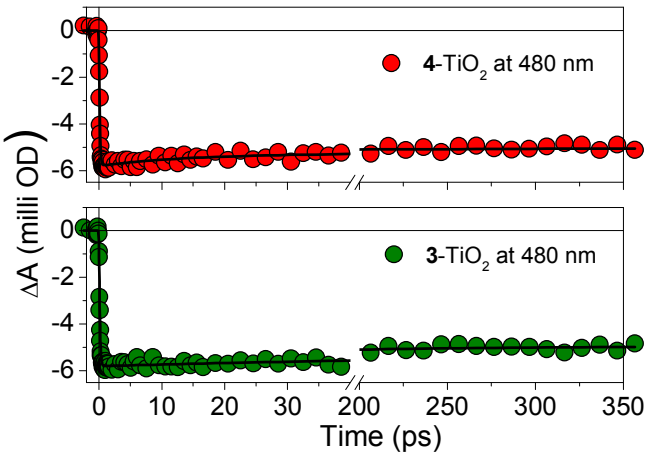

Figure 10: Recovery of the ground state bleach for **3**- and **4**-TiO_2 systems.

The decay of the electron signal at 1000 nm for **5**- and **6**-TiO_2 systems[4] were fitted bi-exponentially with time constants of 4.2 ps (17.1%), > 400 ps (82.9%) and 2 ps (27%), 20 ps (5.4%), > 400 ps (67.6%), respectively. Thus, a comparison of the rate of the decay of this electron signal for the *gem-dicarboxy* and the acetylacetone bound dyes reveals slower backward electron transfer rates in both of our newly designed acetylacetone bound ruthenium(II)- and osmium(II)-polypyridyl systems. Though the electron signal at 1000 nm cannot be designated as the true recombination, one can assume that this slow backward electron transfer in **3**-/**4**-TiO_2 systems is due to a greater separation of the metal centre from the TiO_2 surface than that in **5**-/**6**-TiO_2 systems (*vide supra*).

Conclusion:

New Ru(II)-/Os(II)-polypyridyl based sensitizer having pendent acetylacetone functionality for covalent binding to the nanoparticulate surfaces are synthesized. Time-resolved asorption studies with femtosecond time domain have been carried out for both complexes in water as well as in TiO_2 dispersion in water following excitation with 400 nm laser source. The electron injection process can be found to be fitting with two time constants, a pulse width

limited < 120 fs component and a slower 1.4 ps component for **3**-TiO_2 and a 1.2 ps component for **4**-TiO_2 systems. Unlike other sensitizer molecule where chromophoric centre is separated from anchoring functionality by multiple saturated C-C linkers, the electron injection rate is found to be very fast, which is attributed to a through space electron injection process. The experimental observation is rationalized based on the computational studies with relatively smaller spatial distance between the dye LUMO and the TiO_2 surface. Results in the present studies have also compared with the analogous complexes having *gem-dicarboxy* group as the anchoring functionality for covalent binding to TiO_2 surface in order to compare the role of binding functionalities on electron transfer dynamics. In spite of multiple saturated C-C linkers in complex **3** and **4** fast electron injection and very slow backward electron transfer rate was observed. This is thus expected to contribute in gaining a better insight and thus, help in the future development of highly efficient dyes for use in regenerative dye sensitized solar and aqueous photoelectrochemical fuel cells.

Acknowledgements:

HNG thanks Dr. D. K. Palit and Dr. B. N. Jagatap of Bhabha Atomic Research Centre of Mumbai for their encouragement and continuous support. Financial support for this work is provided BRNS, MNRE/CSIR (through TAP-SUN program) and MSM-CSIR for financial support. T.B. acknowledges CSIR for a Sr. Research Fellowship. A.K.B. thanks UGC for a research fellowship.

Supporting Information Available

Experimental details of Femtosecond Transient absorption spectrometer, Synthesis of TiO2 nanoparticles and Transient absorption spectra for radical cations of **3** and **4**, generated through one electron oxidation by pulse radiolysis are reported in Supporting Information. This material is available free of charge via Internet at http://pubs.rsc.org.

References:

1. (a) M. K. Nazeeruddin, F. De Angelis, S. Fantacci, A. Selloni, G. Viscardi, P. Liska, S. Ito, B. Takeru, M. Gratzel, *J. Am. Chem. Soc.* 2005, **127,** 16835. (b) A. Yella, H.-W. Lee, H. N. Tsao, C. Yi, A. K. Chandiran, M. K. Nazeeruddin, E. W.-G. Diau, C.-Y. Yeh, S. M. Zakeeruddin, M. Gratzel, *Science* 2011, **334,** 629. (c) N. Robertson, *Angew. Chem., Int. Ed.* 2006, **45,** 2338. (d) A. Hagfeldt, G. Boschloo, L. Sun, L. Kloo, H. Pettersson, *Chem. Rev.* 2010, **110,** 6595. (e) R. Argazzi, N. Y. M. Iha, H. Zabri, F. Odobel, C. A. Bignozzi, *Coord. Chem. Rev.* 2004, **248,** 1299. (f) R. Ghanem, Y. Xu, J. Pan, T. Hoffmann, J. Andersson, T. Po- livka, T. Pascher, S. Styring, L. Sun, V. Sundstrom, *Inorg. Chem.* 2002, **41,** 6258.

2. (a) K. Kalyanasundaram, M. Gratzel, *Coord. Chem. Rev.* 1998, **77,** 347. (b) C. She, J. Guo, S. Irle, K. Morokuma, D. L. Mohler, H. Zabri, F. Odobel, K.-T. Youm, F. Liu, J. T. Hupp, T. Lian, *J. Phys. Chem. A* 2007, **111**, 6832. (c) G. Ramakrishna, D. A. Jose, Krishna D. Kumar, A. Das, D. K. Palit, H. N. Ghosh, *J. Phys. Chem. B* 2005, **109,** 15445. (d) T. Banerjee, S. Kaniyankandy, A. Das, H. N. Ghosh, *Inorg. Chem*. 2013, **52,** 5366 and references therein. (e) T. A. Heimer, S. T. D'Arcangelis, F. Farzad, J. M. Stipkala, G. J. Meyer, *Inorg. Chem.* 1996, **35,** 5319. (f) W. R. McNamara, R. C. Snoeberger III, G. Li, C. Richter, L. J. Allen, R. L. Milot, C. A. Schmuttenmaer, R. H. Crabtree, G. W. Brudvig, V. S. Batista, *Energy Environ. Sci.*, 2009, **2,** 1173. (g) P. K. Ghosh, T. G. Spiro, *J. Am. Chem. Soc.* 1980, **102,** 5543.

3. (a) W. R. McNamara, R. C. Snoeberger III, G. Li, J. M. Schleicher, W. C. Cady, M. Poyatos, C. A. Schmuttenmaer, R. H. Crabtree, G. W. Brudvig, V. S. Batista, *J. Am. Chem. Soc.* 2008, **130,** 14329. (b) D. Xiao, L. A. Martini, R. C. Snoeberger III, R. H. Crabtree, V. S. Batista, *J. Am. Chem. Soc.* 2013, **133,** 9014. (c) T. L. Bahers, T. Pauporte, F. Labat, G. Lefevre, I. Ciofini, *Langmuir*, 2011, **27,** 3442. (d) J. Warnan, V.-M. Guerin, F. B. Anne, Y. Pellegrin, E. Blart, D. Jacquemin, T. Pauporté, F. Odobel, *J. Phys. Chem. C* 2013, **117,** 8652. (e) J.-H. Olivier, A. Haefele, P. Retailleau, R. Ziessel, *Org. Lett.* 2010, **12**, 408. (f) W. J. Youngblood, S.-H. A. Lee, Y. Kobayashi, E. A. Hernandez-Pagan, P. G. Hoertz, T. A. Moore, A. L. Moore, D. Gust, T. E. Mallouk, *J. Am. Chem. Soc.* 2009, **131**, 926–927.

4. T. Banerjee, A. K. Biswas, U. G. Reddy, T. S. Sahu, B. Ganguly, A. Das, H. N. Ghosh, *J. Phys. Chem. C* 2014, **118***,* 3864.

5. B. P. Sullivan, D. J. Salmon, T. J. Meyer, *Inorg. Chem.* 1978, **17,** 3334.

6. E. M. Kober, J. V. Caspar, B. P. Sullivan, T. J. Meyer, *Inorg. Chem.* 1988, 27, 4587.

7. (a) M. K. Nazeeruddin, S. M. Zakeeruddin, K. Kalyanasundaram, *J. Phys. Chem.* 1993, **97,** 9607. (b) V. V. Pavlishchuk, A. W. Addison, *Inorg. Chim. Acta* 2000, **298,** 97.

8. K. Sreejith, S. Rawalekar, S. Verma, H. N. Ghosh, *Phys. Chem. Chem. Phys.* 2010, **12,** 4210.

9. V. V. Matylitsky, M. O. Lenz, J. Wachtveitl, *J. Phys. Chem. B* 2006, **110,** 8372.

10. (a) *Materials Studio* DMOL3 Version 4.1, Accelrys Inc., San Diego, CA. (b) B. *J.* Delley, *Chem. Phys.* 2000, **113,** 7756.

11. (a) Z. Wu, R. E. Cohen, D. Singh, *J. Phys. Rev. B* 2004, **70,** 104112. (b) P. Ziesche, S. Kurth, J. P. Perdew, *Comput. Mater. Sci.* 1998, **11,** 122. (c) W. Kohn, A. D. Becke, R. G. Parr, *J. Phys. Chem*. 1996, **100,** 12974.

12. (a) A. Klamt, COSMO and COSMO-RS. In *Encyclopedia of Computational Chemistry*; P. von Rague Schleyer, N. L. Allinger, Eds.; Wiley: New York, **1998**; Vol. *2*, p 604. (b) A. Klamt, *J. Phys. Chem*. 1995, **99,** 2224.

13. Y. Inada, H. Orita, *J Comput Chem* 2008*,* **29**, 225.

14. H. Kusama, H. Orita, H. Sugihara, *Langmuir*, 2008, **24**, 4411.

15. (a) P. C. Redfern, P. Zapol, L. A. Curtiss, T. Rajh, M. C. Thurnauer, *J. Phys. Chem. B* 2003, **107***,* 11419. (b) S. Kaniyankandy, S. Rawalekar, A. Sen, B. Ganguly, H. N. Ghosh, *J. Phys. Chem. C* 2012, **116,** 98.

14. T. Banerjee, S. Rawalekar, A. Das, H. N. Ghosh, *Eur. J. Inorg. Chem.* 2011, 4187.

15. D. Duonghong, J. Ramsden, M. Gratzel, *J. Am. Chem. Soc.* 1982, **104***,* 2917.

16. J. Pan, Y. Xu, G. Benko, Y. Feyziyev, S. Styring, L. Sun, B. Akermark, T. Polivka, V. Sundstrom, *J. Phys. Chem. B* 2004, **108**, 12904.

17. Y. Tachibana, J. E. Moser, M. Gratzel, D. R. Klug, J. R. Durrant, *J. Phys. Chem.* 1996, **100,** 20056.

18. (a) S. Verma, P. Kar, A. Das, H. N. Ghosh, *Chem. Eur. J.* 2011, **17,** 1561. (b) S. Verma, P. Kar, T. Banerjee, A. Das, H. N. Ghosh, *J. Phys. Chem. Lett.* 2012, **3,** 1543.

19. (a) T. Banerjee, S. Kaniyankandy, A. Das, H. N. Ghosh, *J. Phys. Chem. C* 2013, **117,** 3084. (b) T. Banerjee, A. Das, H. N. Ghosh, *New J. Chem.* 2013, **37**, 3100-3108.

20. A. Cannizo, F. V. Mourik, W. Gawelda, G. Zgrablic, C. Bressler, M. Chergui, *Angew. Chem.* 2006, **118,** 3246; *Angew. Chem., Int. Ed.* 2006, **45,** 3174.

21. N. H. Damrauer, J. K. McCusker, *J. Phys. Chem. A* 1999, **103,** 8440.

22. (a) R. A. Malone, D. F. Kelley, *J. Chem. Phys.* 1991, **95,** 8970. (b) J. D. Henrich, H. Zhang, P. K. Dutta, B. Kohler, *J. Phys. Chem. B* 2010, **114,** 14679.

23. (a) S. Wallin, J. Davidsson, J. Modin, L. Hammarstrom, *J. Phys. Chem. A* 2005, **109,** 4697. (b) A. El Nahhas, A. Cannizzo, F. van Mourik, A. M. Blanco-Rodriguez, S. Zalis, Jr. A. Vlcek, M. Chergui, *J. Phys. Chem. A* 2010, **114,** 6361.

24. G. Ramakrishna, D. A. Jose, D. Krishna Kumar, A. Das, D. K. Palit, H. N. Ghosh, *J. Phys. Chem. B* 2005, **109,** 15445.

25. P. Kar, T. Banerjee, S. Verma, A. Sen, A. Das, B. Ganguly, H. N. Ghosh, *Phys. Chem. Chem. Phys.* 2012, **14,** 8192.

26. S. Ardo, G. J. Meyer, *Chem. Soc. Rev.* 2009, **38,** 115.

27. J. Teuscher, J.-D. Decoppet, A. Punzi, S. M. Zakeeruddin, J.-E. Moser, M. Gratzel, *J. Phys. Chem. Lett.* 2012, **3,** 3786.

28. (a) G. Benko, J. Kallioinen, J. E. I. Korppi-Tommola, A. P. Yartsev, V. *J.* Sundstrom, *Am. Chem. Soc.* 2002, **124,** 489. (b) J. Kallioinen, G. Benko, V. Sundstrom, J. E. I. Korppi-Tommola, A. P. Yartsev, *J. Phys. Chem. B* 2002, **106,** 4396.

29. B. Wenger, M. Gratzel, J.-E. Moser, *J. Am. Chem. Soc.* 2005, **127**, 12150.

30. C. She, J. Guo, S. Irle, K. Morokuma, D. L. Mohler, H. Zabri, F. Odobel, K.-T. Youm, F. Liu, J. T. Hupp, T. Lian, *J. Phys. Chem. A* 2007, **111,** 6832.

31. J. B. Asbury, E. Hao, Y. Wang, T. Lian, *J. Phys. Chem. B*, 2000, **104,** 11957.

32. (a) L. Luo, C.-W. Chang, C.-Y. Lin, W.-G. E. Diau, *Chem. Phys. Lett.* 2006, **432,** 452. (b) R. Argazzi, A. R. Chiarati, M. T. Indelli, F. Scandola, C. A. Bignozzi, Book of Abstracts L-09, Eleventh International Conference on Photochemical Conversion and Storage of Solar Energy, Bangalore, India, **1996**. (c) C.-W. Chang, C. K. Chou, I-J. Chang, Y.-P. Lee, E. W.-G. Diau, *J. Phys. Chem. C* 2007**, 111***,* 13288. (d) H. Imahori, S. Kang, H. Hayashi, M. Haruta, H. Kurata, S. Isoda, S. E. Canton, Y. Infahsaeng, A. Kathiravan, T. Pascher, P. Chabera, A. P. Yartsev, V. Sundstrom, *J. Phys. Chem. A* 2011, **115,** 3679.

TOC Abstract and text:

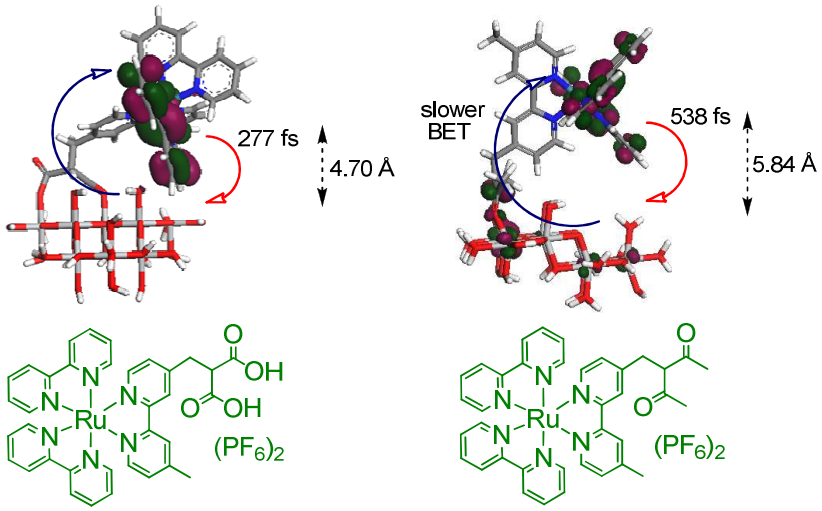

Two new Ru(II)- and Os(II)-polypyridyl based sensitizer dyes have been synthesized with acetylacetone anchoring group for binding of the dye to TiO_2. The *dye-spacer-anchor* arrangement leads to extremely fast through space charge injection rates in addition to the expected slow backward electron transfer.